

Article

Optimum Arrangement of TADAS Dampers for Seismic Drift Control of Buildings Using Accelerated Iterative Methods

Zongjing Li *, Junle Wang, Chen Li and Jing Cao

College of Civil and Transportation Engineering, Hohai University, Nanjing 210098, China

* Correspondence: lizongjing@hhu.edu.cn

Abstract: Triangular added-damping-and-stiffness (TADAS) dampers are reliable passive control devices for earthquake-excited buildings. The arrangement of TADAS dampers in buildings is essentially the allocation of triangular energy dissipation plates (TEDPs) among different stories, which directly influence the passive control effect and the construction cost. This paper proposes four iterated methods to achieve the optimum arrangement of TADAS dampers for seismic drift control of buildings, including the regular iterative method (RIM), the accelerated iterative method (AIM), and two modified accelerated iterative methods (MAIM-I and MAIM-II). Typical high-rise and low-rise buildings are used as application examples to evaluate their performance. Results of the study indicate that the two modified accelerated iterative methods are the most cost-efficient methods for achieving the optimum arrangement of TADAS dampers. This may be attributed to their two-stage implementation mechanism, which combines the set-by-set strategy and the one-by-one strategy in a reasonable way. Additionally, the modified accelerated iterative methods can be especially advantageous for high-rise buildings.

Keywords: TADAS damper; optimum arrangement; iterative methods; passive control



Citation: Li, Z.; Wang, J.; Li, C.; Cao, J. Optimum Arrangement of TADAS Dampers for Seismic Drift Control of Buildings Using Accelerated Iterative Methods. *Buildings* **2023**, *13*, 2720. <https://doi.org/10.3390/buildings13112720>

Academic Editor: Michele Palermo

Received: 26 September 2023

Revised: 20 October 2023

Accepted: 25 October 2023

Published: 28 October 2023



Copyright: © 2023 by the authors. Licensee MDPI, Basel, Switzerland. This article is an open access article distributed under the terms and conditions of the Creative Commons Attribution (CC BY) license (<https://creativecommons.org/licenses/by/4.0/>).

1. Introduction

As a natural disaster, an earthquake may pose a great threat to human beings [1,2]. Researchers around the world have investigated various ways to protect building structures against earthquakes, such as enhancing the strength, ductility, and collapse resistance of structures [3–5] or utilizing active and passive control technologies [6–8]. In recent years, passive control technology, which utilizes dampers to dissipate earthquake input energy, has been well acknowledged by the industry as a growing trend for the seismic design of buildings. According to different mechanisms of energy dissipation, dampers can be categorized into viscous fluid, viscoelastic solid, friction, and metallic dampers, which dissipate energy through fluid orificing, viscoelastic solid deformation, frictional sliding, and yielding of metal.

After decades of research and application, metallic dampers have been shown to be advantageous due to their low cost, simple structure, long-term reliability, stable hysteretic behavior, etc. Therefore, they are particularly preferred by structural engineers in civil engineering applications. Triangular added-damping-and-stiffness (TADAS) dampers are typical metallic dampers used for passive control, which dissipate energy through the yielding of multiple pieces of parallel triangular steel plates. Tsai et al. [9] conducted theoretical and experimental studies on TADAS dampers and provided suggestions for the seismic design of buildings with TADAS dampers. Mahmoudi and Abdi [10] evaluated overstrength, ductility, and response modification factors in special moment-resisting frames with TADAS dampers. Saeedi et al. [11] investigated the seismic behavior and the global damage parameter of moment-resisting frames equipped with TADAS dampers. Tahamouliroudsari et al. [12] experimentally investigated the effect of using TADAS dampers in retrofitting RC moment-resisting frames. Mohammadi et al. [13] studied the performance of TADAS

dampers in very large deformations. Li and Shu [14] improved the detailed structure of TADAS dampers and compared the cyclic performance of TADAS dampers manufactured with regular steel and low-yield-point steel. Akbari Hamed et al. [15] proposed novel multi-level TADAS dampers. Youssef et al. [16] utilized TADAS dampers at a beam–wall interface to enhance the energy dissipation and bearing capacity of a post-tensioned hybrid coupled shear wall system.

The optimum design and assessment of civil structures using smart algorithms and methods has been a research hotspot in recent years [17–21]. For buildings equipped with passive control dampers, the optimum design is essentially the optimum arrangement of dampers within the building. Many researchers have employed smart algorithms such as evolutionary algorithms to solve this problem. Moreschi and Singh (2003) [22] adopted the genetic algorithm (GA) to obtain the optimum arrangement of metallic and friction dampers in seismic-excited buildings. Wongprasert and Symans (2004) [23] employed GA to achieve the optimum distribution of viscous dampers in a 20-story building subject to earthquake loading. Lavan and Dargush (2009) [24] used a multi-objective GA to solve the optimum arrangement of dampers for buildings under seismic excitation. Yousefzadeh et al. (2011) [25] utilized GA to determine the distribution of TADAS dampers considering cost and structural damage. Kim et al. (2017) [26] employed GA in the optimum arrangement of steel plate slit dampers for the seismic retrofit of a reinforced concrete building. Huang (2018) [27] evaluated the effectiveness of GA in optimizing the arrangement of viscous dampers in steel frames under strong earthquakes. Li and Shu (2019) [28] used a modified GA to achieve the optimum placement of metallic dampers for the seismic upgrading of multistory buildings. Amini and Ghaderi (2013) [29] proposed a hybrid AntHS algorithm for the optimum arrangement of structural dampers. Sonmez et al. (2013) [30] utilized the artificial bee colony algorithm (ABCA) to determine the optimum arrangement of viscous dampers in planar buildings.

The above evolutionary algorithms are well capable of handling the optimum arrangement of dampers in seismic-excited buildings. However, the computation process of these algorithms can be highly time-consuming, which may seriously influence the efficiency of the structural design, and the implementation process of these algorithms can be quite sophisticated, which may not be apprehended easily by practicing engineers. In order to provide efficient and practical solutions for structural engineers in the seismic design of buildings equipped with TADAS dampers, this paper proposes accelerated iterative methods to achieve the optimum arrangement of TADAS dampers for seismic drift control of buildings, which are easily implemented and computationally efficient.

The remainder of the paper is organized as follows. Section 2 introduces the structure of a TADAS damper. Section 3 elaborates on the optimum arrangement problem to be solved. Section 4 proposes accelerated iterative methods. Section 5 presents application examples to verify the proposed methods, and the results are discussed in Section 6. Finally, conclusions are provided in Section 7.

2. TADAS Damper

The structure of a typical TADAS damper is shown in Figure 1, which consists of the upper part and the lower part. A TADAS damper may contain multiple pieces of triangular energy dissipation plate (TEDP), whose upper end is welded to the end plate, and the lower end is welded to the pin. Therefore, the TEDP is fixed at the upper end and pinned at the lower end. When the TADAS damper deforms horizontally during earthquakes, the bending curvature of the TEDP is uniform over the full height so that yielding is spread almost uniformly throughout the material, which helps to avoid concentrations of yielding and premature failure. TADAS dampers are usually installed in buildings with stiff bracings, as shown in Figure 2.

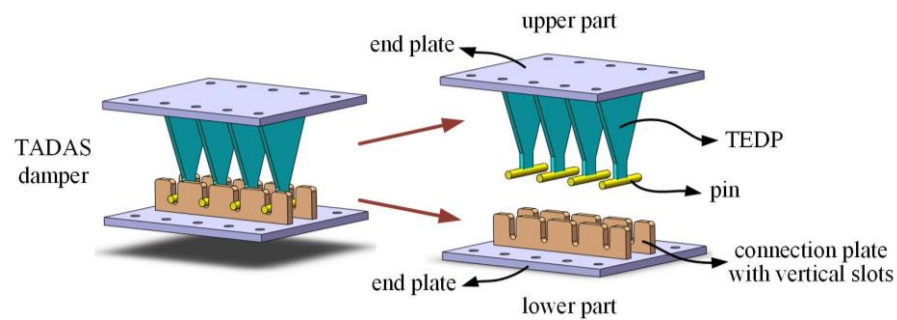


Figure 1. Structure of TADAS damper.

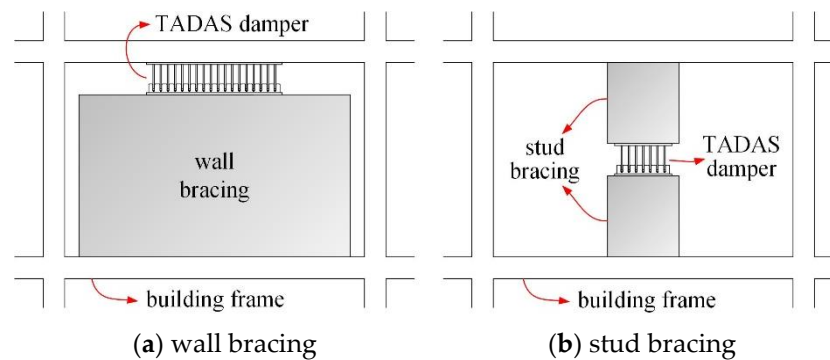


Figure 2. Installation of TADAS damper.

The hysteresis behavior of TEDPs can be described by the bilinear model [10,11]. For a single piece of TEDP, the elastic stiffness k_p , post-yield stiffness k'_p , yield force f_{py} , and yield displacement u_{py} can be obtained by the following equations [9]:

$$k_p = \frac{Ebt^3}{6h^3}, \quad (1)$$

$$k'_p = \gamma k_p, \quad (2)$$

$$f_{py} = \frac{\sigma_y bt^2}{6h}, \quad (3)$$

$$u_{py} = \frac{f_y h^2}{Et}, \quad (4)$$

where E and σ_y are the Young modulus and yield strength of steel; h , b , and t are the height, width, and thickness of TEDPs, respectively; and γ is the post-yield stiffness ratio, which is around 2~3%.

The TEDPs are connected in parallel in the TADAS damper. Therefore, if a TADAS damper consists of N pieces of TEDPs, its elastic stiffness k_d , post-yield stiffness k'_d , yield force f_{dy} , and yield displacement u_{dy} can be obtained by the following equations:

$$k_d = \frac{NEbt^3}{6h^3}, \quad (5)$$

$$k'_d = \gamma k_d, \quad (6)$$

$$f_{dy} = \frac{N\sigma_y bt^2}{6h}, \quad (7)$$

$$u_{dy} = \frac{f_y h^2}{Et}, \quad (8)$$

3. Problem Description

3.1. Analytical Model

The analytical model of a shear-type building equipped with TADAS dampers is shown in Figure 3, where the main structure is represented by an MDOF system with masses lumped at each floor level, and the TADAS dampers at each story are represented by the bilinear models. Define n as the total number of stories in the building and m_i , k_i , and c_i as the mass, stiffness, and inherent damping of the i -th story, respectively. k_{di} , k'_{di} , f_{dyi} , and u_{dyi} are the elastic stiffness, post-yield stiffness, yield force, and yield displacement of the TADAS damper in the i -th story, respectively.

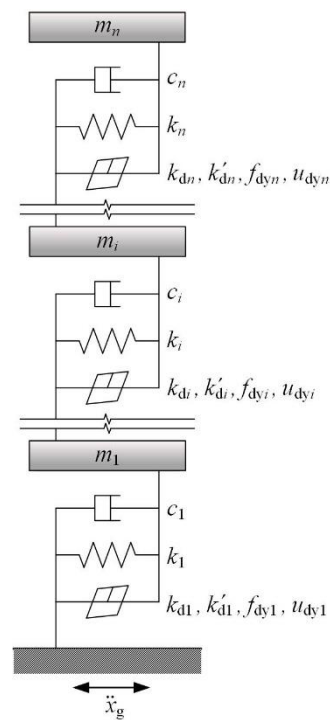


Figure 3. Analytical model of a building with TADAS dampers.

The governing equation of motion for the structural system can be expressed as

$$M\ddot{x} + C\dot{x} + Kx + Hf = -MI\ddot{x}_g, \quad (9)$$

where M , K , and C represent the mass, stiffness, and inherent damping matrices, respectively; x , \dot{x} , and \ddot{x} are vectors representing the displacement, velocity, and acceleration of the structure; \ddot{x}_g represents the earthquake ground acceleration; I is a vector with all elements being unity; and H is a matrix given by:

$$H = \begin{bmatrix} 1 & -1 & & & & & \\ & 1 & -1 & & & & \\ & & 1 & \ddots & & & \\ & & & \ddots & -1 & & \\ & & & & 1 & -1 & \\ & & & & & 1 & \\ & & & & & & 1 \end{bmatrix}, \quad (10)$$

$f = (f_1, \dots, f_i, \dots, f_n)$ is a vector representing the restoring force provided by the TADAS dampers in the building, where the i -th element f_i represents the restoring force provided by the TADAS dampers in the i -th story. Assuming that the TADAS damper in the i -th story consists of N_i TEDPs, k_{di} , k_{di}' , F_{dyi} , and u_{dyi} can be calculated using Equations (5)–(8) so that the bilinear model used to describe f_i can be obtained.

3.2. Optimization Problem

As the TADAS damper consists of multiple pieces of TEDPs, the optimum arrangement of TADAS dampers in a building is essentially the optimum distribution of TEDPs among different stories. Assuming that the TADAS damper in the i -th story consists of N_i pieces of TEDPs, the arrangement of TEDPs in the building can be represented by the vector $d = [N_1, \dots, N_n]$.

The interstory drift ratio indicates potential damage to the structure and thus is a key factor for structural safety. Seismic design codes in many countries have stipulated the allowable limit for the interstory drift ratio. For example, the Chinese Code for Seismic Design of Buildings (GB50011-2010) [31] has proposed the allowable interstory drift ratio limits in the performance-based design guidelines. Another key factor we need to consider in practical design is the cost of construction projects. In this study, TADAS dampers are used to enhance the seismic performance of building structures so that the cost can be represented by the total number of TEDPs used in the building. Therefore, combining the above two key factors, the design is preferable if we can use fewer TEDPs to achieve the allowable interstory drift ratio limit.

By defining the optimal arrangement of TEDPs as $d_{\text{opt}} = [N_1, \dots, N_n]_{\text{opt}}$, the total number of TEDPs as N_{sum} , the maximum interstory drift ratio of the building as θ_{max} and the allowable interstory drift ratio limit as θ_{lim} , the optimization problem to be solved in this paper can be simply expressed as find d_{opt} which utilizes the minimum N_{sum} to achieve $\theta_{\text{max}} \leq \theta_{\text{lim}}$.

4. Solution Methods

For a building equipped with TADAS dampers, there may be hundreds or even more TEDPs distributed in different stories of the building, whose optimum arrangement can be a large-scale discrete optimization problem. The computational cost to solve such problems can be quite high for evolutionary algorithms such as GA, which may seriously undermine their feasibility in practical engineering.

In order to solve the above optimization problem efficiently, four iterative methods are proposed in this section, namely the regular iterative method (RIM), the accelerated iterative method (AIM), the modified accelerated iterative method I (MAIM-I), and the modified accelerated iterative method II (MAIM-II).

Define θ_{lim} as the allowable interstory drift ratio limit and θ_i as the peak interstory drift ratio of the i -th story so that the peak interstory drift ratios of the building can be represented by $\theta = [\theta_1, \dots, \theta_n]$. In this study, θ is obtained by nonlinear time-history analysis (NTHA) of the building. θ_{max} is the maximum interstory drift ratio among all stories of the building, and i_{max} is the corresponding story number, which can be obtained by the function $[\theta_{\text{max}}, i_{\text{max}}] = \max(\theta)$. Similarly, θ_{min} is the minimum interstory drift ratio among all stories of the building, and i_{min} is the corresponding story number, which can be obtained by the function $[\theta_{\text{min}}, i_{\text{min}}] = \min(\theta)$. It should be noted that the stories with no TEDPs should be excluded when searching for θ_{min} . j denotes the number of iterations. The arrangement of TEDPs in the building varies with iterations, which can be represented by the distribution vector $d_j = [N_{1-j}, \dots, N_{n-j}]$, where N_{i-j} denotes the number of TEDPs in the i -th story at the j -th iteration. For the original building without a damper, the distribution vector is initialized as $d_0 = [0, \dots, 0]$. For the optimum solution, the optimized distribution vector is denoted by d_{opt} . The proposed methods and flowcharts are presented as follows.

4.1. Regular Iterative Method (RIM)

In the regular iterative method (RIM), the distribution vector is first initialized as $d_0 = [0, \dots, 0]$ for the original building, and nonlinear time-history analysis (NTHA) is conducted for the building. Then, a piece of TEDP is added to the i_{\max} -th story, and the distribution vector d_j is updated by increasing 1 in the i_{\max} -th element. NTHA is conducted for the updated building. As long as $\theta_{\max} \leq \theta_{\lim}$ is not satisfied, one more piece of TEDP is added to the i_{\max} -th story of the current building, with d_j updated and NTHA performed accordingly. The iteration terminates once $\theta_{\max} \leq \theta_{\lim}$ is satisfied, and the final d_j is taken as the optimum solution d_{opt} . The flowchart of RIM is presented in Figure 4.

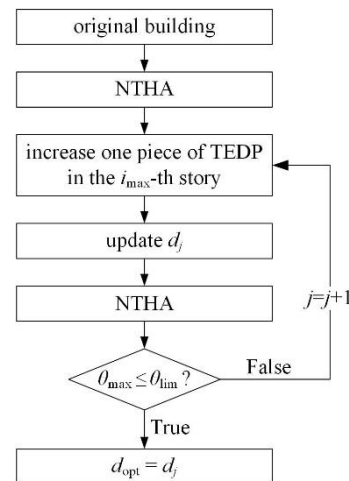


Figure 4. Flowchart of RIM.

4.2. Accelerated Iterative Method (AIM)

The buildings (especially high-rise buildings) may need a large amount of TEDPs to achieve the allowable interstory drift ratio limit. Therefore, the one-by-one strategy used by RIM can be quite slow. In order to improve the computational efficiency, the accelerated iterative method (AIM) is proposed based on a set-by-set strategy. The difference between AIM and RIM is that AIM adds multiple pieces of TEDPs as a set to the building in each iteration, while RIM adds only one piece of TEDP to the building in each iteration. Theoretically, if AIM adds Q pieces of TEDPs as a set in each iteration, its computational efficiency is Q times faster than RIM. However, the set-by-set strategy is likely to bring redundant TEDPs to the structural system, especially when Q is relatively large. The flowchart of AIM is presented in Figure 5.

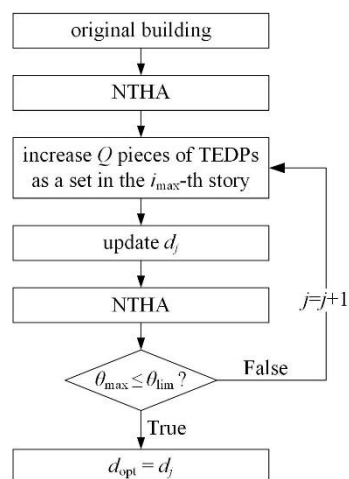


Figure 5. Flowchart of AIM.

4.3. Modified Accelerated Iterative Method I (MAIM-I)

Although AIM may converge significantly faster, it may bring redundant TEDPs to the structural system. If proper measures can be taken to remove the redundant TEDPs, the results obtained by AIM can be effectively refined. Based on this idea, the modified accelerated iterative method I (MAIM-I) is proposed.

As shown in Figure 6, MAIM-I is implemented using a two-stage procedure. In the first stage, AIM is implemented which adds multiple pieces of TEDPs as a set to the i_{\max} -th story at each iteration until $\theta_{\max} \leq \theta_{\lim}$ is satisfied. At the end of the first stage, d' as a near-optimum solution with redundant TEDPs is obtained. In the second stage, one piece of TEDP is reduced in the i_{\min} -th story at each iteration until $\theta_{\max} \leq \theta_{\lim}$ is no longer satisfied, and the previous solution d_{j-1} which still satisfies $\theta_{\max} \leq \theta_{\lim}$ is defined as d_- . Then, in order to prevent premature convergence, one piece of TEDP is added in the i_{\max} -th story, and the current solution is defined as d_+ . If $d_+ \neq d_-$, the solution goes back for further adjustment. If $d_+ = d_-$, the iteration should be terminated so as to avoid getting into infinite cycles.

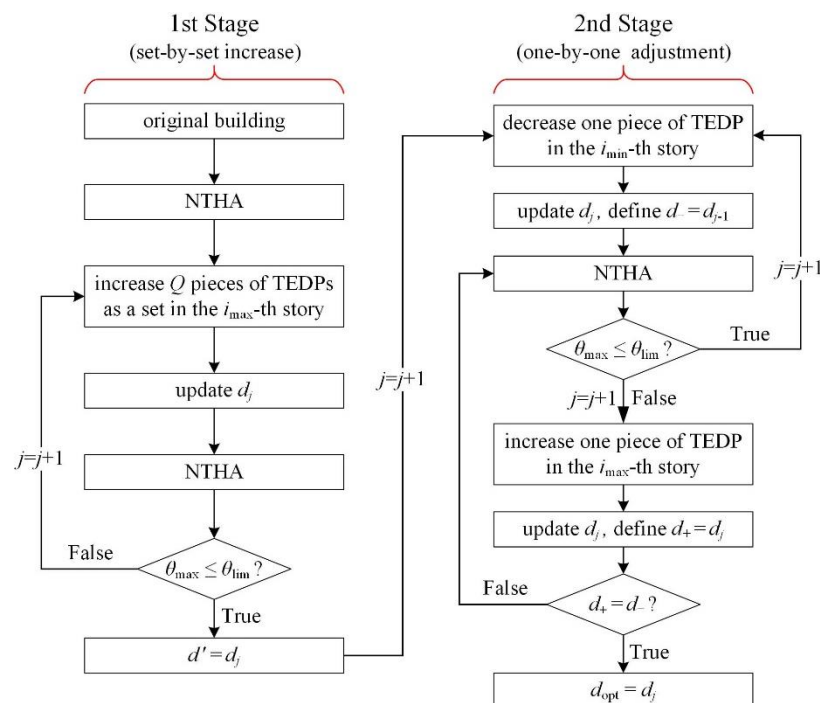


Figure 6. Flowchart of MAIM-I.

Therefore, in MAIM-I, the first stage is a fast increase procedure using set-by-set strategy which reaches an intermediate solution with redundant TEDPs efficiently, while the second stage is a slow adjustment procedure using one-by-one strategy which refines the solution by removing redundant TEDPs.

4.4. Modified Accelerated Iterative Method II (MAIM-II)

Another way to improve AIM is to combine AIM and RIM in a reasonable way. In the beginning when θ_{\max} is far from θ_{\lim} , AIM can be employed to efficiently achieve a near-optimum solution with insufficient TEDPs. Then, RIM can be used when θ_{\max} gets near θ_{\lim} so that the number of TEDPs increases slowly afterwards and less redundant TEDPs are brought to the structural system in the end. Based on this idea, the modified accelerated iterative method II (MAIM-II) is proposed.

As shown in Figure 7, MAIM-II is implemented using a two-stage procedure. In the first stage, multiple pieces of TEDPs as a set are added to the i_{\max} -th story of the building in each iteration until $\theta_{\max} \leq \theta_{\lim+}$ is satisfied, where $\theta_{\lim+}$ is slightly larger than θ_{\lim} . At the end of the first stage, d'' as an intermediate solution with insufficient TEDPs is obtained.

In the second stage, only one piece of TEDP is added to the i_{\max} -th story of the building in each iteration until $\theta_{\max} \leq \theta_{\lim}$ is finally satisfied, and the last solution is taken as the optimum solution d_{opt} .

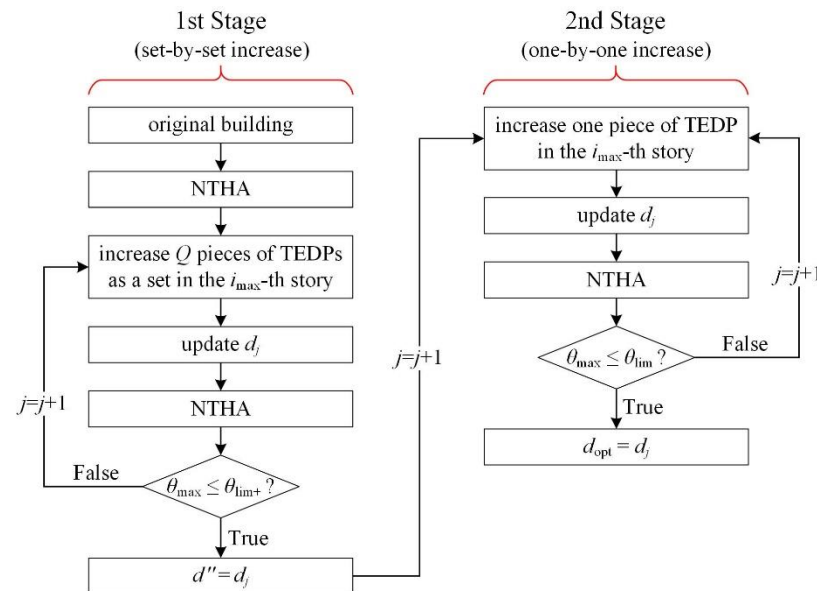


Figure 7. Flowchart of MAIM-II.

Therefore, in MAIM-II, the first stage is a fast increase procedure using the set-by-set strategy, which reaches an intermediate solution with insufficient TEDPs efficiently, while the second stage is a slow increase procedure using the one-by-one strategy which approaches the final optimum solution with better precision.

5. Application Example

In order to evaluate the proposed methods, two buildings are presented in this section as the original buildings. Building 1 is a typical high-rise building with 20 stories. The structural model of Building 1 is transformed into a simplified 20-degrees-of-freedom (20-DOF) system, whose story height, story stiffness k , and story mass m are $[h_1, \dots, h_{20}] = [3.9, 3.6, 3.6, 3.6, 3.6, 3.6, 3.6, 3.6, 3.6, 3.6, 3.6, 3.6, 3.6, 3.6, 3.6, 3.6, 3.6, 3.6, 3.6, 3.6]$ m, $[k_1, \dots, k_{20}] = [1.04, 1.02, 1.00, 0.99, 0.98, 0.85, 0.83, 0.82, 0.81, 0.80, 0.66, 0.65, 0.64, 0.63, 0.62, 0.49, 0.48, 0.47, 0.46, 0.43] \times 10^5$ kN/m, and $[m_1, \dots, m_{20}] = [178, 178, 178, 178, 176, 174, 174, 174, 174, 174, 173, 173, 173, 173, 172, 171, 171, 171, 171, 169]$ t, respectively. Building 2 is a typical low-rise building with six stories. The structural model of Building 2 is transformed into a simplified six-degrees-of-freedom (6-DOF) system, whose story height, story stiffness k , and story mass m are $[h_1, \dots, h_6] = [3.9, 3.6, 3.6, 3.6, 3.6, 3.6]$ m, $[k_1, \dots, k_6] = [0.58, 0.55, 0.53, 0.42, 0.41, 0.40] \times 10^5$ kN/m, and $[m_1, \dots, m_6] = [172, 172, 171, 170, 170, 169]$ t, respectively. Rayleigh damping is adopted for the structural models.

In this study, three earthquake ground motions are selected to perform the NTHAs according to the Chinese Code for Seismic Design of Buildings (GB50011-2010), including two recorded ground motions and one artificial ground motion, and the maximum response value is computed. PGA of the ground motions is scaled to 0.4g according to the Chinese Code. As shown in Figure 8, the mean spectrum of the selected ground motions is compatible with the design spectrum. The key parameters of the TEDPs are set as $k_p = 4000$ kN/m, $k_p' = 0.02k_p$, $u_{py} = 0.002h_i$, $f_{py} = k_p \cdot u_{py}$, and the geometry of the TEDPs can be obtained through Equations (1)–(4). The allowable interstory drift ratio limit is set as $\theta_{\lim} = 0.008$.

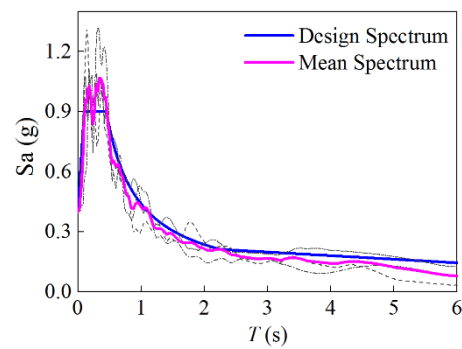


Figure 8. Spectra of earthquake ground motions. The hyphen lines represent the individual spectra of the three selected earthquake ground motions.

5.1. Building 1

Optimum story-wise arrangements of TEDPs in Building 1 obtained by different methods are shown in Table 1, where N_{sum} is the total number of TEDPs in the building, which indicates the quality of the solution, and j_{max} is the total number of iterations, which indicates the computation efficiency of the method. As shown, RIM achieved the best solution with 456 TEDPs, which was the least among the four methods. However, it took 456 iterations to converge. Considering that three NTHAs were required in each iteration, RIM needed 1368 NTHAs to yield the solution, whose computational cost was quite high. On the other hand, AIM only took 97 iterations to yield the solution, which was far more efficient. However, AIM yielded a less satisfactory solution using 485 TEDPs to achieve the allowable interstory drift ratio limit, which was the most among the four methods. MAIM-I and MAIM-II have yielded solutions similar to the solution yielded by RIM, while they only took 126 and 116 iterations to converge, which was about 1/4 the computational cost of RIM. Obviously, MAIM-I and MAIM-II are able to yield good solutions efficiently, achieving the balance between efficiency and quality.

Table 1. Optimum arrangements of TEDPs in Building 1 obtained by proposed methods.

Story	RIM	AIM	MAIM-I	MAIM-II
20	0	0	0	0
19	0	0	0	0
18	0	0	0	0
17	3	5	3	3
16	9	10	9	10
15	7	10	7	6
14	16	15	16	16
13	24	25	24	25
12	29	30	29	30
11	35	35	35	35
10	30	30	30	30
9	34	35	34	34
8	36	35	35	36
7	36	40	36	36
6	35	40	36	36
5	28	30	28	28
4	31	35	32	31
3	35	35	35	35
2	38	40	39	38
1	30	35	31	31
N_{sum}	456	485	459	460
j_{max}	456	97	126	116

The interstory drift ratios of Building 1 with different arrangements of TEDPs obtained by the proposed methods are presented in Figure 9. As shown, the allowable interstory

drift ratio limit can be achieved by adopting any of the TEDP arrangements obtained by the four proposed methods. Moreover, the interstory drift ratios obtained by RIM, MAIM-I, and MAIM-II are almost identical and are uniformly distributed over the height of the building, while the interstory drift ratios obtained by AIM are smaller than those obtained by the other methods in some of the stories. The iteration curves are plotted in Figure 10. Evidently, AIM, MAIM-I, and MAIM-II were a lot more efficient than RIM. Among them, MAIM-I and MAIM-II took only a few more iterations than AIM, but in exchange, they yielded solutions similar to the best solution produced by RIM, which were quite cost-efficient.

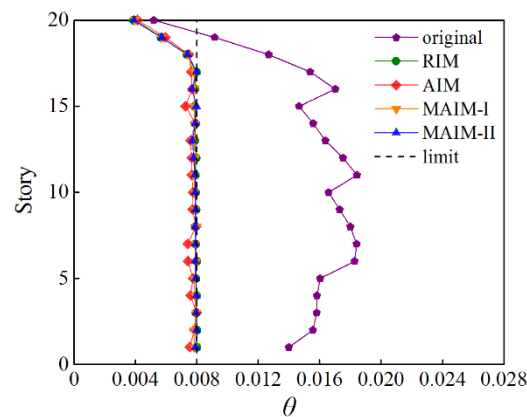


Figure 9. Distribution of interstory drift ratio (Building 1).

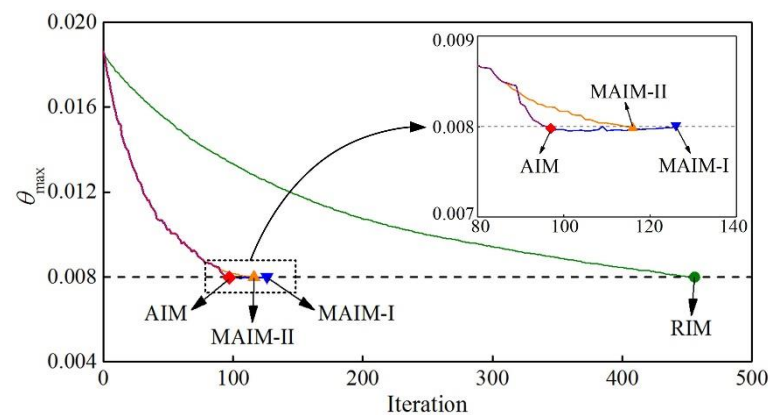


Figure 10. Iteration curves (Building 1).

5.2. Building 2

Optimum story-wise arrangements of TEDPs in Building 2 obtained by different methods are shown in Table 2. As shown, RIM, MAIM-I, and MAIM-II achieved the best or comparable solutions, and AIM required a few more TEDPs in the solution. However, it is observed that there is no significant difference among the solutions obtained by these methods. In terms of computational efficiency, the proposed methods can be ranked as RIM, MAIM-II, MAIM-I and AIM, which took 13, 20, 22, and 59 iterations to converge, respectively. Although the computational cost varies, the overall computational cost for Building 2 is considerably lower than Building 1.

The interstory drift ratios of Building 2 with different arrangements of TEDPs obtained by the proposed methods are presented in Figure 11. As shown, the allowable interstory drift ratio limit can be achieved by adopting any of the TEDP arrangements obtained by the four proposed methods. Moreover, the interstory drift ratios obtained by RIM, MAIM-I, and MAIM-II are almost identical and are uniformly distributed over the height, while the interstory drift ratios obtained by AIM are smaller than those obtained by the other

methods in some of the stories. The iteration curves are plotted in Figure 12. It is shown that AIM was the most efficient while RIM was the least efficient. MAIM-I and MAIM-II required a few more iterations than AIM to achieve refined solutions.

Table 2. Optimum arrangements of TEDPs in Building 2 obtained by proposed methods.

Story	RIM	AIM	MAIM-I	MAIM-II
6	0	0	0	0
5	3	5	3	4
4	9	10	9	10
3	5	5	5	4
2	18	20	18	17
1	24	25	24	25
N_{sum}	59	65	59	60
j_{max}	59	13	22	20

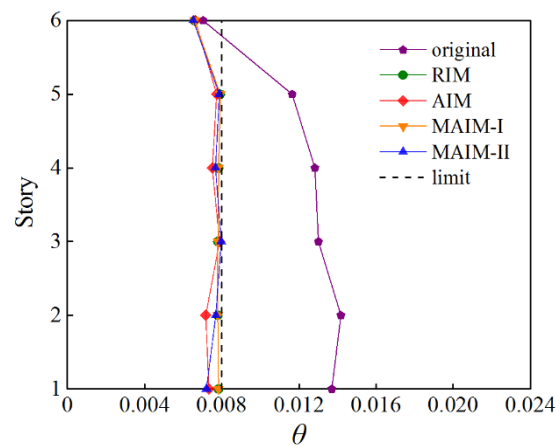


Figure 11. Distribution of interstory drift ratio (Building 2).

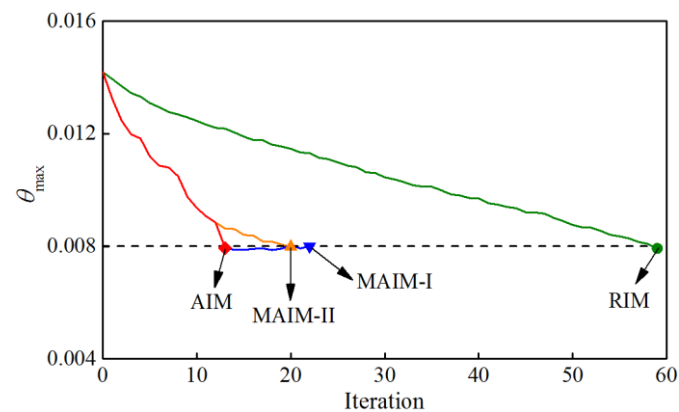


Figure 12. Iteration curves (Building 2).

6. Discussion

6.1. Comparison of Applicability

Building 1 and Building 2 represent typical high-rise and low-rise buildings with story stiffness increasing from top to bottom. A summary of the optimum TEDP arrangement results for both building models obtained by the proposed methods is listed in Table 3. As shown, for both building models, RIM obtains the best solutions but is the least efficient, while AIM is on the contrary. MAIM-I and MAIM-II can obtain the best or close to best solutions with only a little extra computational cost than AIM, which are the most cost-efficient methods.

Table 3. Results summary.

		RIM	AIM	MAIM-I	MAIM-II
Building 1	N_{sum}	456	485	459	460
	j_{max}	456	97	126	116
Building 2	N_{sum}	59	65	59	60
	j_{max}	59	13	22	20

Furthermore, the high-rise building needs a lot more TEDPs to achieve the allowable interstory drift ratio limit than the low-rise building so that the computational cost is higher than low-rise buildings. In Building 1, the computational cost of MAIM-I and MAIM-II is about 1/4 computational cost of RIM, which can save 330~340 iterations than RIM. On the other hand, In Building 2, although the computational cost of MAIM-I and MAIM-II is about 1/3 computational cost of RIM, they only saved about 37~39 iterations than RIM, which is significantly smaller than that of Building 1. Therefore, the difference in computational cost among different methods is relatively smaller for low-rise buildings, while it can be considerably larger for high-rise buildings. It is highly recommended to use MAIM-I and MAIM-II for high-rise buildings because they can be especially advantageous in such cases.

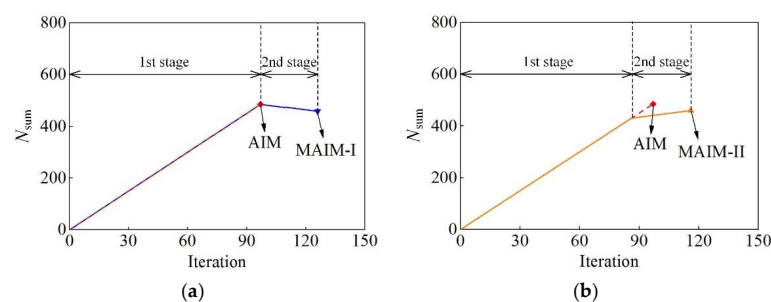
6.2. Comparison of Mechanism

A comparison of implementation mechanisms among the proposed methods is presented in Table 4. As shown, RIM and AIM are one-stage methods, while MAIM-I and MAIM-II are two-stage methods. The advantages of MAIM-I and MAIM-II may be attributed to their two-stage implementation mechanism.

Table 4. Comparison of implementation mechanisms among proposed methods.

	RIM	AIM	MAIM-I	MAIM-II
1st Stage	One-by-one increase	Set-by-set increase	Set-by-set increase	Set-by-set increase
2nd Stage	N/A	N/A	One-by-one adjustment	One-by-one increase

The variation of N_{sum} during iteration of MAIM-I and MAIM-II is illustrated in Figure 13. In their first stage, the set-by-set strategy is employed to efficiently produce an intermediate solution near the optimum one. The only difference is that in MAIM-I, the first stage is identical to AIM, while in MAIM-II, the first stage terminates earlier than AIM. Therefore, at the end of the first stage of MAIM-I, an intermediate solution with excessive TEDPs is obtained, while at the end of the first stage of MAIM-II, an intermediate solution with insufficient TEDPs is obtained. Then, they switch to using the one-by-one strategy so as to reduce the excessive and replenish the insufficient TEDPs in a more accurate manner. Consequently, the solution obtained by the first stage can be further refined in the second stage. The balance between efficiency and quality is thus achieved in MAIM-I and MAIM-II.

**Figure 13.** Variation of N_{sum} during iteration: (a) MAIM-I vs. AIM; (b) MAIM-II vs. AIM.

6.3. Influence of Q

In the first stage of MAIM-I and MAIM-II, Q pieces of TEDPs are added to the building in each iteration. Therefore, Q decides the efficiency of the first stage. For Building 1, the performance of MAIM-I and MAIM-II with different values of Q is compared in Table 5, where j_{1st} and j_{2nd} denote the number of iterations in the first and second stages, respectively. When $Q = 1$, MAIM-I and MAIM-II are equivalent to RIM.

Table 5. Performance of MAIM-I and MAIM-II with different values of Q .

	MAIM-I			MAIM-II		
	$Q = 1$	$Q = 5$	$Q = 10$	$Q = 1$	$Q = 5$	$Q = 10$
N_{sum}	456	459	459	456	460	461
j_{1st}	456	97	53	456	86	39
j_{2nd}	0	29	72	0	30	71
j_{max}	456	126	125	456	116	110

As shown, N_{sum} remains stable when Q is chosen at different values. Therefore, MAIM-I and MAIM-II are capable of adapting to different values of Q . Furthermore, it is observed that for both MAIM-I and MAIM-II, when Q is larger, fewer iterations are needed in the first stage, while more iterations are needed in the second stage. Larger Q means better efficiency but less accuracy in the first stage. Therefore, although a larger value of Q can increase the efficiency of the first stage, it may yield a solution further from the optimum one at the end of the first stage so that more iterations are needed in the second stage to refine the solution.

7. Conclusions

In this paper, four iterative methods, i.e., the regular iterative method (RIM), the accelerated iterative method (AIM), and two modified accelerated iterative methods (MAIM-I and MAIM-II), are proposed to achieve the optimum arrangement of TADAS dampers in earthquake-excited buildings for drift control. Typical high-rise and low-rise buildings are used as application examples to evaluate their performance. Based on the results of the study, the following conclusions can be drawn:

- (1) RIM obtains the best solutions but is the least efficient, while AIM is on the contrary; MAIM-I and MAIM-II can well achieve the balance between efficiency and quality, which are the most cost-efficient methods;
- (2) MAIM-I and MAIM-II can be especially advantageous for high-rise buildings;
- (3) The advantages of MAIM-I and MAIM-II can be attributed to their two-stage implementation mechanism, which combines the set-by-set strategy and the one-by-one strategy in a reasonable way;
- (4) By adopting the optimum arrangement of TADAS dampers, the building can achieve the allowable interstory drift ratio limit with minimum cost.

Author Contributions: Conceptualization, Z.L.; methodology, Z.L.; investigation, Z.L., J.W. and C.L.; validation, J.W., C.L. and J.C.; writing—original draft preparation, Z.L. and J.W.; writing—review and editing, Z.L. and J.C.; funding acquisition, Z.L. All authors have read and agreed to the published version of the manuscript.

Funding: This research was funded by the National Natural Science Foundation of China (NSFC) (Grant No. 52208163) and the Fundamental Research Funds for the Central Universities (Grant No. B230201035).

Data Availability Statement: Not applicable.

Conflicts of Interest: The authors declare no conflict of interest.

References

1. Chen, J.; Wen, L.; Bi, C.; Liu, Z.; Liu, X.; Yin, L.; Zheng, W. Multifractal analysis of temporal and spatial characteristics of earthquakes in Eurasian seismic belt. *Open Geosci.* **2023**, *15*, 20220482. [\[CrossRef\]](#)
2. Wu, M.; Ba, Z.; Liang, J. A procedure for 3D simulation of seismic wave propagation considering source-path-site effects: Theory, verification and application. *Earthq. Eng. Struct. Dyn.* **2022**, *51*, 2925–2955. [\[CrossRef\]](#)
3. Zhang, Q.; Wei, Z.; Gu, X.; Yang, Q.; Li, S.; Zhao, Y. Confinement behavior and stress-strain response of square concrete columns strengthened with carbon textile reinforced concrete (CTRC) composites. *Eng. Struct.* **2022**, *266*, 114592. [\[CrossRef\]](#)
4. Zhang, Q.; Zheng, N.; Gu, X.; Wei, Z.; Zhang, Z. Study of the confinement performance and stress-strain response of RC columns with corroded stirrups. *Eng. Struct.* **2022**, *266*, 114476. [\[CrossRef\]](#)
5. Tian, L.; Li, M.; Li, L.; Li, D.; Bai, C. Novel joint for improving the collapse resistance of steel frame structures in column-loss scenarios. *Thin Walled Struct.* **2023**, *182*, 110219. [\[CrossRef\]](#)
6. Zhang, C. The active rotary inertia driver system for flutter vibration control of bridges and various promising applications. *Sci. China-Technol. Sci.* **2023**, *66*, 390–405. [\[CrossRef\]](#)
7. Soong, T.T.; Spencer, B.F. Supplemental energy dissipation: State-of-the-art and state-of-the-practice. *Eng. Struct.* **2002**, *24*, 243–259. [\[CrossRef\]](#)
8. Lee, C.H.; Ju, Y.K.; Min, J.K.; Lho, S.H.; Kim, S.D. Non-uniform steel strip dampers subjected to cyclic loadings. *Eng. Struct.* **2015**, *99*, 192–204. [\[CrossRef\]](#)
9. Tsai, K.C.; Chen, H.W.; Hong, C.P.; Su, Y.E. Design of steel triangular plate energy absorbers for seismic-resistant construction. *Earthq. Spectra.* **1993**, *9*, 505–528. [\[CrossRef\]](#)
10. Mahmoudi, M.; Abdi, M.G. Evaluating response modification factors of TADAS frames. *J. Constr. Steel Res.* **2012**, *71*, 162–170. [\[CrossRef\]](#)
11. Saeedi, F.; Shabakhty, N.; Mousavi, S.R. Seismic assessment of steel frames with triangular-plate added damping and stiffness devices. *J. Constr. Steel Res.* **2016**, *125*, 15–25. [\[CrossRef\]](#)
12. Tahamouliroudsari, M.; Eslamianesh, M.B.; Entezari, A.R.; Noori, O.; Torkaman, M. Experimental assessment of retrofitting RC moment resisting frames with ADAS and TADAS yielding dampers. *Structures* **2018**, *14*, 75–87. [\[CrossRef\]](#)
13. Mohammadi, R.K.; Nasri, A.; Ghaffary, A. TADAS dampers in very large deformations. *Int. J. Steel Struct.* **2017**, *17*, 515–524. [\[CrossRef\]](#)
14. Li, Z.; Shu, G. Test and evaluation of modified TADAS devices with different grades of steel. *Earthq. Eng. Eng. Vib.* **2020**, *19*, 451–464.
15. Akbari Hamed, A.; Mortazavi, S.F.; Saeidzadeh, M. Evaluation of the seismic performance of structures equipped with novel multi-level TADAS dampers. *Asian J. Civ. Eng.* **2023**, *24*, 969–988. [\[CrossRef\]](#)
16. Youssef, A.A.; Esfahani, M.R.; Zareian, M.S. Experimental evaluation of post-tensioned hybrid coupled shear wall system with TADAS steel dampers at the beam-wall interface. *Structures* **2023**, *53*, 1283–1299. [\[CrossRef\]](#)
17. Xu, J.G.; Feng, D.C.; Mangalathu, S.; Jeon, J.S. Data-driven rapid damage evaluation for life-cycle seismic assessment of regional reinforced concrete bridges. *Earthq. Eng. Struct. Dyn.* **2022**, *51*, 2730–2751. [\[CrossRef\]](#)
18. Sun, J.; Ma, Y.; Li, J.; Zhang, J.; Ren, Z.; Wang, X. Machine learning-aided design and prediction of cementitious composites containing graphite and slag powder. *J. Build. Eng.* **2021**, *43*, 102544. [\[CrossRef\]](#)
19. Sun, J.; Wang, X.; Zhang, J.; Xiao, F.; Sun, Y.; Ren, Z.; Zhang, G.; Liu, S.; Wang, Y. Multi-objective optimisation of a graphite-slag conductive composite applying a BAS-SVR based model. *J. Build. Eng.* **2021**, *44*, 103223. [\[CrossRef\]](#)
20. Sun, J.; Wang, Y.; Yao, X.; Ren, Z.; Zhang, G.; Zhang, C.; Chen, X.; Ma, W.; Wang, X. Machine-learning-aided prediction of flexural strength and ASR expansion for waste glass cementitious composite. *Appl. Sci.* **2021**, *11*, 6686. [\[CrossRef\]](#)
21. Sun, J.; Wang, J.; Zhu, Z.; He, R.; Peng, C.; Zhang, C.; Huang, J.; Wang, Y.; Wang, X. Mechanical performance prediction for sustainable high-strength concrete using bio-inspired neural network. *Buildings* **2022**, *12*, 65. [\[CrossRef\]](#)
22. Moreschi, L.M.; Singh, M.P. Design of yielding metallic and friction dampers for optimal seismic performance. *Earthq. Eng. Struct. Dyn.* **2003**, *32*, 1291–1311. [\[CrossRef\]](#)
23. Wongprasert, N.; Symans, M.D. Application of a genetic algorithm for optimal damper distribution within the nonlinear seismic benchmark building. *J. Eng. Mech.* **2004**, *130*, 401–406. [\[CrossRef\]](#)
24. Lavan, O.; Dargush, G.F. Multi-objective evolutionary seismic design with passive energy dissipation systems. *J. Earthq. Eng.* **2009**, *13*, 758–790. [\[CrossRef\]](#)
25. Yousefzadeh, A.; Sebt, M.H.; Tehranizadeh, M. The optimal TADAS damper placement in moment resisting steel structures based on a cost-benefit analysis. *Int. J. Civ. Eng.* **2011**, *9*, 23–32.
26. Kim, J.; Kim, M.; Eldin, M.N. Optimal distribution of steel plate slit dampers for seismic retrofit of structures. *Steel Compos. Struct.* **2017**, *25*, 473–484.
27. Huang, X. Evaluation of genetic algorithms for the optimum distribution of viscous dampers in steel frames under strong earthquakes. *Earthq. Struct.* **2018**, *14*, 215–227.
28. Li, Z.; Shu, G. Optimal placement of metallic dampers for seismic upgrading of multistory buildings based on a cost-effectiveness criterion using genetic algorithm. *Struct. Des. Tall Spec. Build.* **2019**, *28*, e1595. [\[CrossRef\]](#)
29. Amini, F.; Ghaderi, P. Hybridization of harmony search and ant colony optimization for optimal locating of structural dampers. *Appl. Soft Comput.* **2013**, *13*, 2272–2280. [\[CrossRef\]](#)

30. Sonmez, M.; Aydin, E.; Karabork, T. Using an artificial bee colony algorithm for the optimal placement of viscous dampers in planar building frames. *Struct. Multidiscip. Optim.* **2013**, *48*, 395–409. [[CrossRef](#)]
31. *GB 50011-2010*; National Standard of the People's Republic of China. Code for Seismic Design of Buildings. China Architecture & Building Press: Beijing, China, 2016.

Disclaimer/Publisher's Note: The statements, opinions and data contained in all publications are solely those of the individual author(s) and contributor(s) and not of MDPI and/or the editor(s). MDPI and/or the editor(s) disclaim responsibility for any injury to people or property resulting from any ideas, methods, instructions or products referred to in the content.